

Performance Comparison of Nb and NbN Antenna-coupled Microbolometers*

C. Dietlein^{abd}, A. Luukanen^b, J. S. Penttilä^c, H. Sipola^c, L. Grönberg^c, H. Seppä^c, P. Helistö^c, and
E. N. Grossman^d

^aDept. of Electrical and Computer Engineering, University of Colorado at Boulder, 425 UCB,
Boulder, CO, 80309-0425, USA

^bMillimetre-wave Laboratory of Finland – MilliLab, Tietotie 3, 02044 Espoo, Finland

^cVTT Technical Research Centre of Finland, Tietotie 3, 02044 Espoo, Finland

^dOptoelectronics Division, National Institute of Standards and Technology, 325 Broadway,
Boulder, CO, 80305-3328, USA

ABSTRACT

We report the experimental results of a comparison between free-standing Nb and NbN microbolometer bridges coupled to equiangular spiral antennas on Si substrates. Because of the difference in material resistivity, bolometer resistance and aspect ratio is varied independently. Room-temperature antenna patterns measured at 650 GHz with a backward-wave oscillator are presented, as are I - V curves at $T = 300$ K and at $T = 4$ K. At room temperature, zero-bias resistance and specific responsivity are examined, and at 4 K, normal-state resistance and saturation power are studied. Nb devices display significantly lower saturation powers than NbN devices whose dimensions have been adjusted to provide equal resistance. However, for both materials, the inferred thermal conductances are higher than predicted by the Wiedemann-Franz relation, by approximately a factor of ~ 2 for Nb and a factor of ~ 5 for NbN. In general, and especially for the room-temperature responsivity, the substantial spread in parameters from device to device exceeds any systematic difference in performance between the materials.

Keywords: bolometer, millimeter-wave, terahertz

1. INTRODUCTION

When lithographic antennas were first pioneered for mm-wave and THz applications, simple resistive microbolometers, either freestanding or substrate-supported, were one of the first detectors to be integrated with them. At that time, Bi – a semimetal – was the most commonly used room-temperature bolometer material¹ because it was felt that, for practical bolometer dimensions, metals would provide too low a resistance to efficiently match to typical $\sim 100 \Omega$ antenna impedances, while semiconductors would provide too high an impedance. At film thicknesses of >100 nm, this was indeed a reasonable conclusion, but as thin-film fabrication techniques improved it became straightforward to make much thinner films with good control and reproducibility. Thus, antenna-coupled microbolometers (ACMBs) made from thin (20 nm or less) Nb were demonstrated^{2,3}, while, partly inspired by the development of uncooled infrared microbolometers (which are not antenna-coupled), many other uncooled bolometer materials have also been explored⁴.

One of the original motivations for the use of Nb (versus other high-resistivity metals) was its compatibility with superconducting devices. Nb deposition and patterning techniques, as well as understanding of its properties in thin-film form, were developed quite early because of interest in superconducting devices, particularly tunnel junctions⁵. Thus, the same freestanding antenna-coupled microbolometer structure as used at room-temperature has also been carefully investigated in superconducting mode^{6,7}. In this case, its operation is quite different than at room temperature, because the internal temperature gradients within the bridge are large compared to the width of the superconducting transition, while at room-temperature, the internal temperature gradients are much smaller than the temperature scale over which the resistance changes significantly. These temperature gradients are in both cases created by the dissipation of Joule

*Publication of the U.S. Government; not subject to copyright.

heat in the bridge from the applied bias. In the superconducting case, this Joule heat creates a “hotspot” at the center of the bridge, where the temperature lies above the superconducting transition temperature T_c of the film. This hotspot generates all the DC voltage appearing across the bridge. The detailed theory of detection and mixing in superconducting hotspots has been developed and experimentally verified fairly recently^{8,9}, though it was largely foreshadowed by very early work on the physics of superconducting wires¹⁰.

In any case, the chief parameters governing the operation of an antenna-coupled microbolometer, and characterizing its sensitivity in the two ranges of operating temperature are as follows:

Uncooled

$$\text{Specific responsivity: } \beta = \frac{l}{G} \frac{dR}{dT} \left[\frac{V}{W \cdot mA} \right]$$

$$\text{Zero-bias resistance: } R_0$$

Cryogenic

$$\text{Saturation power: } P_{sat} = G(T_c - T_0)$$

$$\text{Normal-state resistance: } R_n$$

G is the thermal conductance between the bolometer and the heat bath. If the thermal conductivity of the bridge material is relatively constant with temperature, then G is simply given by $G = 12\kappa A/l$, where A , l , and κ are the cross-sectional area, length, and thermal conductivity of the bridge¹¹.

NbN is another material whose development in thin film form was largely stimulated by interest in superconducting devices. It has a somewhat higher transition temperature than pure Nb, though in both cases T_c depends strongly on film thickness as well as internal film stress and other properties controlled by deposition conditions. In its normal state, NbN is a “granular metal”¹² meaning that electronic conduction can be described by a model of grains, each consisting of a standard Drude metal but separated from one another by inter-granular tunneling barriers. The typical grain size can be longer or shorter than the Drude mean free path, depending on deposition conditions; on a macroscopic scale, NbN films have resistivities that are considerably higher than pure Nb and temperature coefficients of resistance (TCR) that can either be positive or negative depending on deposition conditions, similar to semimetals.

The higher resistivity of NbN naturally motivates its investigation as an alternative to Nb for antenna-coupled microbolometers. If the normal-state resistance of the bolometer is held fixed, to match a specific antenna impedance, the difference in material resistivities implies that the NbN bridge will be thicker and/or shorter than its Nb counterpart. This in turn implies a higher T_c and/or a lower inductance, respectively. Theoretically, this inductance can cause a significant loss in overall coupling efficiency at high frequencies.

2. MATERIALS AND GEOMETRIES

2.1 Nb ACMB

The Nb detectors have been described previously^{13,14}. Briefly, a 20 nm x 1 μm x l μm Nb bridge is suspended between the feed-points of a spiral antenna. The length of the bridge, l , determines the high-frequency cutoff of the spiral antenna, and for Nb bridges in this paper is either 12 μm or 24 μm , corresponding to $f_c = 3.6$ THz or 1.8 THz, respectively. The Si substrate beneath the bridge is removed with an isotropic XeF₂ etch, leaving the Nb bridge free-standing. The thermal conductivity of the bridge to the heat bath, G consists of two additive (parallel) components, that due to the Nb bolometer itself and that due to thermal conduction through the SiO₂ that encapsulates the Nb. A rendering of the cross section is seen in Fig. 1. The depth of the XeF₂ etch varies between 5 μm and 12 μm from chip to chip. As the etch windows in the SiO₂ are separated by 4 μm total (2 μm on either side of the centerline of the Nb bridge), the minimum etch depth in order to fully “release” the Nb bridge from the Si substrate is 2 μm . Etch depths greater than 2 μm ensure that the bridge is free-standing, but also remove Si from beneath the inner-most radiating portion of the antenna.

2.2 NbN ACMB

To compensate for the higher resistivity of NbN and present a similar impedance at the antenna feed point, the NbN bridge aspect ratio is changed, increasing both width ($w = 2$ μm) and thickness ($t = 250$ nm). Length l defines antenna bandwidth, and is either $l = 8$ μm (corresponding to $f_c = 5.4$ THz) or $l = 19$ μm . The NbN bridges lie atop SiO₂, but have no SiO₂ on top of them. The Si etch is anisotropic. SEM images of the etched devices show that the etch pit size reduces from the initial etch window size, as depth increases. This anisotropy decreases the under-etch of the inner-most

portion of the antenna, but leaves a vertical Si “fin” standing collinear beneath the NbN bridge, approximately half the height of the total etch depth.

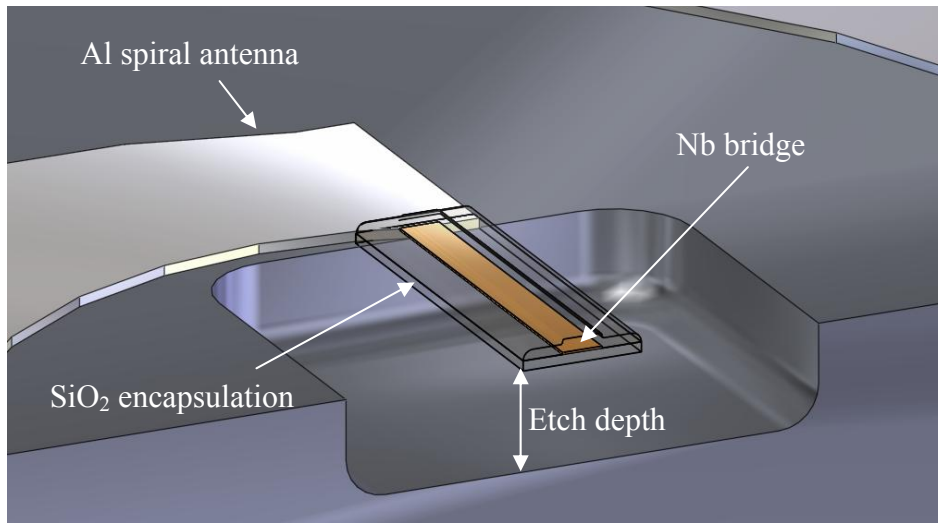


Fig. 1. Cross-section cutaway section rendering of an Nb bridge encapsulated in SiO₂, suspended above Si at the feed-point of a circular spiral antenna. Rendering is simplified and not to scale. In actuality, the Si floor of the etch pit is rough, and the sidewalls of the pit are concave.

3. DESCRIPTION OF THE TEST SETUPS

3.1 Room-temperature electrical and antenna pattern measurements

At 300 K, device I - V curves are measured using a simple current-bias circuit. Bias currents are on the order of several hundred μ A. Device failure occurs above 1 mA, i.e., current density $J > 5 \times 10^6$ A/cm². NbN devices fail at approximately a factor of two greater current than Nb devices, but because of the larger cross-section this corresponds to a lower current density, $J > 5 \times 10^5$ A/cm². I - V curves are measured and the data fit to $V = I(R_o + \beta IV)$, where R_o is the zero-bias resistance of the bridge and β is its normalized electrical responsivity². Additionally, antenna patterns are measured with an azimuth-elevation stage and a backward-wave oscillator (BWO) at $f = 650$ GHz. The beam is mechanically chopped at the BWO horn aperture, and the detector response is monitored with a lock-in amplifier.

3.2 Superconducting electrical measurements

The Nb devices are tested at 4.2 K in a liquid He cryostat. I - V curves and response to a 77 K blackbody are read out by either the room-temperature electronics discussed in¹⁵, or a simple resistive-readout bias circuit. A closed-cycle cryogen-free pulse-tube cryorefrigerator is used for testing the NbN devices at temperatures down to 2.6 K. Multiple device I - V curves are measured simultaneously using a multiple-channel version of the room-temperature electronics.

4. RESULTS

4.1 Room temperature I - V measurements

Table 1 summarizes results of five Nb devices tested at 300 K. The mean zero-bias resistance, R_o , of the $l = 24$ μ m bridges is 483 Ω , while the single Nb bridge with $l = 12$ μ m was fitted to 211 Ω . Specific responsivities for $l = 24$ μ m devices on wafer SC4 are on average 244 V/W/mA, while for wafer SC5, $\beta = 123$ V/W/mA, nearly a factor of two lower than SC4, even though the device geometries are nominally identical. A possible explanation is that film thickness is slightly lower on SC5 than on SC4 (with a slight difference in width so as to maintain R_o constant), since dR/dT is a strong function of film thickness at 20 nm, where the Drude mean free path is comparable to thickness.

Table 2 summarizes the results of ten NbN devices tested at 300 K. Two values of bridge length were tested, $l = 8$ μ m and $l = 19$ μ m. The mean zero-bias resistance, R_o , for the shorter bridges is 185 Ω , and for the longer bridges

Table 1: Room-temperature parameters for Nb devices, extracted from I - V curves fitted to $V = I(R_o + \beta IV)$.

Unique identifier	Bridge length	R_o [Ω]	β [V/W/mA]
Nb SC4 NW #1 cent	12 μm	211.3	80.51
Nb SC4 NE #1 cent	24.5 μm	500.5	266.1
Nb SC4 NE #2 cent	24.5 μm	481.3	221.1
Nb SC5 NE #1 cent	24.5 μm	482.8	122.4
Nb SC5 NE #3 cent	24.5 μm	465.6	123.6

Table 2: Room-temperature extracted parameters for NbN devices.

Unique identifier	Bridge length	R_o [Ω]	β [V/W/mA]
NbN PC05 D1 F12 cent	8 μm	189.3	-53.3
NbN PC05 D1 F12 cor1	8 μm	183.1	-49.67
NbN PC05 D1 F12 cor2	8 μm	183.3	-60.54
NbN PC05 D1 D8 cent	8 μm	191.6	-56.45
NbN PC05 D1 F10 cent	8 μm	179.8	-49.8
NbN PC05 D1 E7 cent	8 μm	184.8	-55.92
NbN PC05 D3 C8 cent	18.8 μm	409.9	-157
NbN PC05 D3 C8 cor1	18.8 μm	447.9	-183.5
NbN PC05 D3 C8 cor2	18.8 μm	434.7	-178.4
NbN PC05 D3 C6 cent	18.8 μm	460.8	-203.8

$R_o = 439 \Omega$. The difference in resistance corresponds exactly to the factor of 2.375 between the two bridge lengths. Noted is that responsivity is negative, due to the negative TCR of NbN.

The mean specific responsivity for bridges of length $l = 8 \mu\text{m}$ is $\beta = -54 \text{ V/W/mA}$, while for bridges of length $l = 19 \mu\text{m}$, the mean responsivity is $\beta = -181 \text{ V/W/mA}$. The specific responsivity for NbN devices thus lies approximately midway between the values seen for the Nb devices from the two separate, nominally identical wafers. It is noted that NbN bridges can be biased at higher currents, therefore achieving greater effective responsivity, and that the TCR for these devices was not optimized for 300 K.

4.2 Room-temperature antenna patterns

Due to the low transmit power of the BWO providing irradiance on the order of several $\mu\text{W}/\text{mm}^2$ at the plane of the detector, the dynamic range in most of the measurements is not greater than 22 dB. Measured patterns produced similar results in terms of -3 dB beamwidths and sidelobe levels. Examples of typical antenna patterns taken at $f \approx 650 \text{ GHz}$ are shown in Fig. 2. Incident radiation is coupled to the antenna via a hyper-hemispherical Si substrate lens on the back of the chip, centered over a device on the opposing side. The diameter of the lens is 4 mm.

4.3 Superconducting I - V measurements

In the limit of zero optical power (P_{opt}) dissipated in the bridge – the small-signal limit – the superconducting I - V curves

for Nb and NbN bridges are given by $I(V) = V/R_n + P_{sat}/V$, where $P_{sat} = \frac{V_{min}^2}{R_n}$, with V_{min} the voltage at the minimum

in the I - V curve. Hot-spot superconducting bridge responsivity is simply $-1/2V_{min}$. Therefore, devices with lower saturation power are theoretically more sensitive.

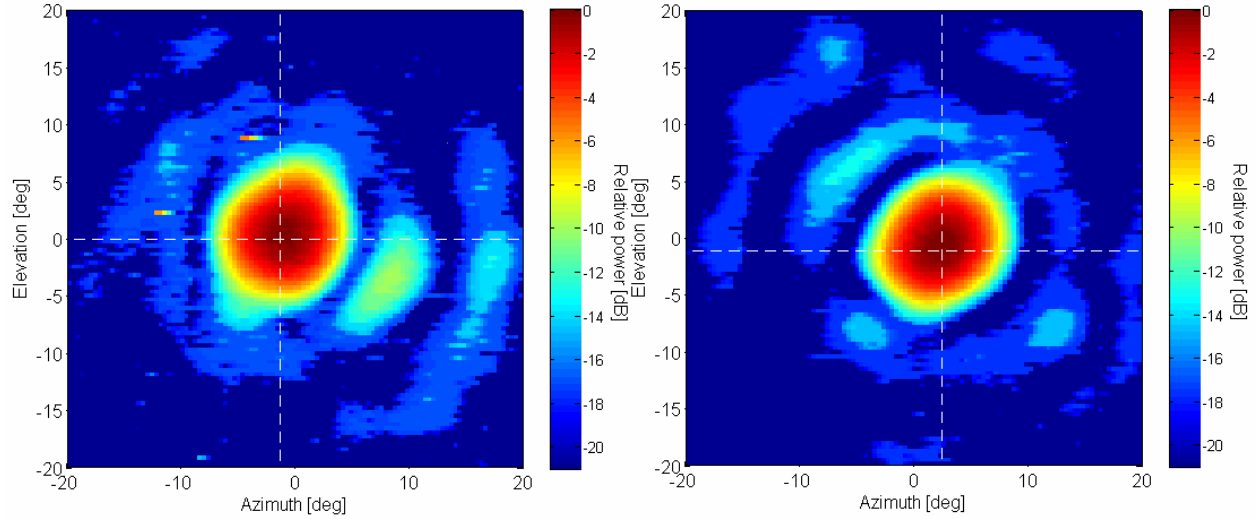


Fig. 2. Antenna patterns of Nb (left) and NbN (right) devices at $f \approx 650$ GHz. The incident field is linearly polarized with the electric field in the elevation plane. The bolometer axis is in the azimuth direction. The -3 dB beamwidths for the Nb device are 6.7° in azimuth and 6.6° in elevation, and for the NbN device, 6.7° in azimuth and 6.8° in elevation. First sidelobe levels are approximately -9 dB – -11 dB.

Table 3 summarizes the fitted parameters R_n , P_{sat} , and P_{opt} (if optical power was incident on the detector) for Nb bridge I - V curves measured at 4.2 K. The Nb devices tested at superconducting temperatures are coupled to antennas with high-frequency cutoffs of $f_c = 1.8$ THz or 3.6 THz, corresponding to bridge lengths of either $l = 24$ μm or $l = 12$ μm , respectively. The nominal antenna low-frequency cutoff is 200 GHz, although operation below 200 GHz occurs due to bias traces on the Si substrate extending from the arms of the spiral in a dipole-like manner. The mean normal-state resistance, R_n , of the superconducting $l = 24$ μm Nb bridges is 217 Ω . Superconducting Nb bridges of length $l = 12$ μm have normal-state resistances on average of $R_n = 113$ Ω . Bridges of that length that did *not* superconduct had normal-state resistances on average of 348 Ω . The mean saturation power for $l = 24$ μm bridges is 16.9 nW, ignoring the outlier SC4 1x8 1.8 THz SW (2), and for $l = 12$ μm bridges is 37.4 nW.

Table 3: Fitted parameters for Nb devices at $T = 4.2$ K. Fits including optical power (P_{opt}) are used when the detector is exposed to incident radiation from outside the cryostat.

Unique identifier	Fit parameters			R_n [Ω] lin. fit $T < T_c$
	R_n [Ω]	P_{sat} [nW]	P_{opt} [nW]	
Nb SC4 1x8 1.8 THz SW (2)	226	6.31	n/a	n/a
Nb SC4 1x8 1.8 THz SW (3)	242	16.5		
Nb SC4 1x8 1.8 THz SW (5)	199	18.9		
Nb SC4 1x8 1.8 THz SW (6)	190	13.4		
Nb SC4 3.6 THz #1 (0,0) light	113	37.7	9.6	114
" " dark	115	34.4	3.3	118
Nb SC4 3.6 THz #4 (0,0) light	112	39.1	4.2	115
" " dark	112	38.5	2.1	115
Nb SC4 1.8 THz #2 (1,1) light	227	18.9	5.5	254
Nb SC5 1.8 THz #2 (0,0)	n/a			380
Nb SC5 1.8 THz #3 (1,1)	n/a			315

Table 4 summarizes four measured superconducting NbN bridges. All superconducting tests were performed on NbN devices of bridge length $l = 8 \mu\text{m}$. As these devices were tested in a cryorefrigerator enabling control of detector temperature, R_n values were also obtained by increasing T to greater than T_c ($\sim 12 \text{ K}$), and measuring I - V curves. Finding R_n in this method is generally more reliable than performing linear fits to the normal region of an I - V curve when $T < T_c$. The mean normal-state resistance of these bridges at approximately 3.8 K is 283Ω , extracted from the superconducting fit. A linear fit to the normal region of the I - V curve produces an average R_n , with the single outlier (D8 (-1,-1)) ignored, of 293Ω , while the R_n measured from I - V curves when $T > T_c$ is on average 290Ω . The mean saturation power of the NbN devices is $P_{sat} = 113 \text{ nW}$ (outlier ignored).

Table 4: Fitted parameters for NbN devices. In addition to the R_n fits from I - V curves measured at 4 K , R_n was measured above T_c .

Unique identifier	Fit parameters			R_n [Ω] lin. fit $T < T_c$	R_n [Ω] lin. fit $T > T_c$
	R_n [Ω]	P_{sat} [nW]	P_{opt} [nW]		
NbN PC05 D1 F8 (0,0)	234	123	26	282	275
NbN PC05 D1 F8 (-1,-1)	265	111	21	299	n/a
NbN PC05 D1 D8 (0,0)	283	112	-1.2	304	309
NbN PC05 D1 D8 (-1,-1)	383	80	n/a	389	n/a

Examples of typical measured I - V curves for Nb and NbN devices are shown in Fig. 3. A clear difference exists between the Nb and NbN devices in saturation power, with the Nb devices exhibiting values a factor of ~ 5 lower than those of NbN devices whose bridge dimensions have been adjusted to give approximately equal normal-state resistance.

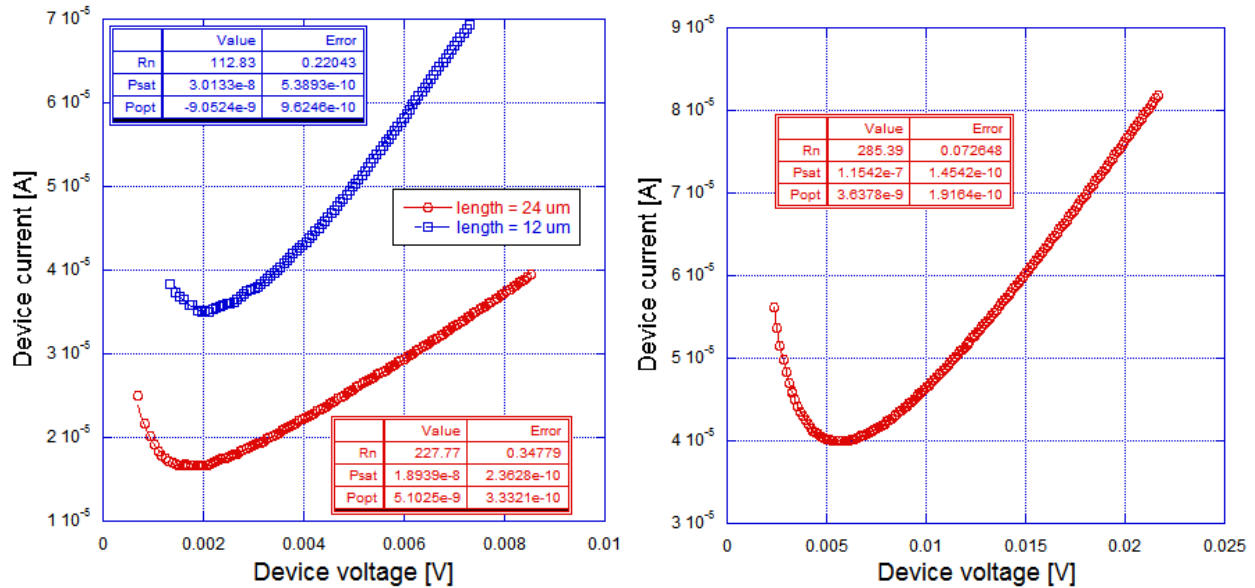


Fig. 3. (left) Examples of typical superconducting Nb I - V curves for bridge lengths of $l = 12 \mu\text{m}$ and $l = 24 \mu\text{m}$. V_{min} is approximately 1.5 - 2.0 mV for both devices, while the normal-state resistance R_n is a function of bridge length. Saturation power for the shorter bridge is higher than the longer bridge by a factor of 1.6 . (right) A typical NbN I - V curve with bridge length $l = 8 \mu\text{m}$. Saturation power is approximately 115 nW , in the normal range for measured NbN devices; V_{min} is approximately 5.5 mV .

5. DISCUSSION

Room-temperature testing revealed that although differences in zero-bias resistance and responsivity are found between Nb and NbN devices, the measurement spread of Nb responsivity between wafers is greater than any systematic difference in performance between the materials. Thus a definitive conclusion regarding performance at 300 K of the different materials is not reached. Antenna patterns are, as expected, not functions of bolometer material but of the antenna and substrate lens.

Table 5 provides typical parameters of the measured devices at 4 K. The measured thermal conductance is obtained by dividing the saturation power by the difference in superconducting transition temperature and base temperature. Though T_c is not routinely measured for either set of devices, spot measurements indicate $T_c \sim 6.5$ K for the Nb devices and $T_c \sim 11.5$ K for the NbN devices. The reliability of T_c values is questionable, but the fact that $(T_c - T_o)$ is several degrees larger for NbN than for Nb is certain.

Table 5: Comparison of relevant superconducting Nb and NbN parameters. For the Wiedemann-Franz value of thermal conductance G_{w-f} , L_o is the Lorenz number, G_{elec} is the electrical conductivity ($1/R_n$), and T is the mean bridge temperature.

	Nb	NbN
R_n	220 Ω ($l = 24 \mu\text{m}$)	295 Ω ($l = 8 \mu\text{m}$)
P_{sat}	17 nW	120 nW
$T_c - T_o$	$\sim 3^*$	$\sim 8.5^*$
$G_{meas} = P_{sat}/(T_c - T_o)$	5.7 nW/K	14.1 nW/K
$G_{w-f} = 4L_oTG_{elec}$	2.5 nW/K	2.6 nW/K

*Measurement of T_c was not systematic, and is less accurate than the other measured parameters in this table.

The discrepancy between the measured thermal conductance G and the value obtained by the Wiedemann-Franz relation can be explained by introducing a parallel G . In both the Nb and NbN devices, the additive G stems from both phonon conduction in the metal and thermal conduction through the SiO_2 , either encapsulating the bridge (Nb) or lying under it (NbN). While the ratio of these contributions is not known, the encapsulating SiO_2 is likely the dominant parallel G for the 20-nm thin-film Nb bridges, while phonon conduction most likely dominates the parallel G for the NbN devices with cross-sectional area a factor of 25 higher than Nb.

In conclusion, we find that at room temperature, the data do not provide a definitive answer regarding superiority of one material over the other, due to the spread of Nb responsivity between devices from the two wafers tested. At superconducting temperatures, Nb devices are more sensitive, following from their lower saturation power. However, we realize that this performance difference is not significant in most systems, where many other factors play greater roles in overall system performance.

6. ACKNOWLEDGEMENTS

The U.S. authors acknowledge the support of the Department of Homeland Security Directorate for Science and Technology, NSF interdisciplinary award #0501578, and thank Zoya Popović for extensive helpful discussions. The Finnish authors acknowledge Tekes decision #40384/05.

REFERENCES

1. D. P. Neikirk, Lam, W.W., and Rutledge, D.B., "Far-infrared Microbolometer Detectors," *Int. J. of Ir and Mm-Waves*, vol. 5, pp. 245-277, 1984.
2. M. E. MacDonald, Grossman, E. N., "Niobium Microbolometers for Far-infrared Detection," *IEEE Trans. on Microwave Theory and Techniques*, vol. 43, pp. 893-896, 1995.
3. A. Rahman, deLange, G., Hu, Q., "Micromachined Room-temperature Microbolometers for Millimeter-wave Detection," *Appl. Phys. Lett.*, vol. 68, pp. 2020-2022, 1996

4. R. A. Wood, "Monolithic Silicon Microbolometer Arrays," in *Uncooled Infrared Imaging Arrays and Systems*, vol. 47, *Semiconductors and Semimetals*, P. W. Kruse and D. D. Skatrud, Eds. San Diego: Academic Press, 1997, pp. 43-122.
5. M. Gurvitch, M. A. Washington, and H. A. Huggins, "High-quality refractory Josephson tunnel junctions utilizing thin aluminum layers," *Appl. Phys. Lett.*, vol. 42, pp. 472-474, 1983.
6. A. Luukanen, E. N. Grossman, A. J. Miller, P. Helistö, J. S. Penttilä, H. Sipola, and H. Seppä, "An ultra-low noise superconducting antenna-coupled microbolometer with a room-temperature readout," *IEEE Microw. Wirel. Compon. Lett.*, vol. 16, pp. 464-466, 2006.
7. A. Luukanen, "High performance microbolometers and microcalorimeters: from 300 K to 100 mK," Ph.D. thesis, Department of Physics, University of Jyväskylä, 2003.
8. D. W. Floet, J. J. A. Baselmans, T. M. Klapwijk, and J. R. Gao, "Resistive transition of niobium superconducting hot-electron bolometer mixers," *Appl. Phys. Lett.*, vol. 73, no. 19, pp. 2826-2828, 1998.
9. D. W. Floet, E. Miedema, T. M. Klapwijk, and J. R. Gao, "Hotspot mixing: A framework for heterodyne mixing in superconducting hot-electron bolometers," *Appl. Phys. Lett.*, vol. 74, no. 3, pp. 433-435, 1999.
10. W. J. Skocpol, M. R. Beasley, and M. Tinkham, "Self-heating hotspots in superconducting thin-film microbridges," *J. Appl. Phys.*, vol. 45, pp. 4054-4066, 1974.
11. D. P. a. R. Neikirik, D.B., "Air-bridge Microbolometer for Far-infrared Detection," *Appl. Phys. Lett.*, vol. 44, pp. 153-155, 1984.
12. A. Nigro, Nobile, G., Rubino, M.G., and Vaglio, R., "Electrical Resistivity of Polycrystalline Niobium Nitride Films," *Phys. Rev. B.*, vol. 37, pp. 3970-3972, 1988.
13. A. J. Miller, A. Luukanen, and E. N. Grossman, "Micromachined antenna-coupled uncooled microbolometers for terahertz imaging arrays," *Proc. SPIE*, vol. 5411, pp. 18-24, 2004.
14. A. Luukanen and J. P. Pekola, "A superconducting antenna-coupled hot-spot microbolometer," *Appl. Phys. Lett.*, vol. 82, pp. 3970-3972, 2003.
15. J. S. Penttilä, H. Sipola, P. Helistö, and H. Seppä, "Low-noise readout of superconducting bolometers based on electrothermal feedback," *Supercond. Sci. Technol.*, vol. 19, pp. 319-322, 2006.